Author's Version

Increasing the oxidation resistance of γ-TiAl by applying a magnetron sputtered aluminum and silicon based coating

Peter-Philipp Bauer[1], Nadine Laska[1], Radosław Swadźba[2]

[1]German Aerospace Center (DLR), Institute of Materials Research, Linder Hoehe, D-51147 Cologne, Germany,

[2]Łukasiewicz Research Network - Institute for Ferrous Metallurgy, Gliwice, Poland

Intermetallics (2021)
https://doi.org/10.1016/j.intermet.2021.107177

Increasing the oxidation resistance of γ-TiAl by applying a magnetron sputtered aluminum and silicon based coating

Peter-Philipp Bauer[1], Nadine Laska[1], Radosław Swadźba[2]

[1]German Aerospace Center (DLR), Institute of Materials Research, Linder Hoehe, D-51147 Cologne, Germany,

[2]Łukasiewicz Research Network - Institute for Ferrous Metallurgy, Gliwice, Poland

Abstract:

In this study, the suitability of a magnetron sputtered Al-18Si (at.%) coating as oxidation protection for a γ-TiAl based TNB-V2 alloy was investigated. The coating microstructure and its changes as well as the evolution of the different phases during the different steps, deposition process, post heat treatment and isothermal oxidation test, was studied using x-ray diffraction as well as scanning and transmission electron microscopy.

The well adherent coating provides a homogenous, dense and crack free crystalline microstructure of Si grains in an Al matrix. The phase evolution analysis during a 20 h post-heat treatment at 550 °C with *in situ* x-ray diffraction reveals the complete formation of the $TiAl_3$ phase due to the reaction of Ti from the TNB-V2 substrate and Al from the coating. During oxidation at 850 °C for 300 h, a thermally grown α-Al_2O_3 layer was formed providing excellent oxidation resistance. The formation of α-Al_2O_3 relies on the presence of $TiAl_3$ whereas the silicon acted as a getter for Ti and thus could prevent the formation of TiO_2. Furthermore, the finally formed Ti_5Si_3 phase reduces the inwards diffusion of Al into the substrate and prevents fast Al depletion in the coating. Moreover, the hierarchical coating microstructure, consisting of a $TiAl_3$ matrix with a network-like structure of the Ti_5Si_3 phase, could be beneficial in terms of mechanical properties.

1. Introduction

γ-TiAl intermetallics offer a high specific strength which makes them attractive for light-weight applications [1-3]. Additionally, they show a good oxidation resistance below 800 °C [4-6]. Therefore, they are an attractive material for rotating components in aircraft engines to substitute nickel-based alloys. Today, the GEnx™ and LEAP™ engines are equipped with the TiAl-based alloy Ti-48Al-2Cr-2Nb (in at.%) in the last two stages of the low pressure turbine [7]. Pratt & Whitney's PW1000G-JM engine utilizes the Mo-containing γ-TiAl alloy TNM in the low pressure turbine as well [8].

Current efforts are being made to further increase the oxidation resistance and thus to increase the service temperature or the lifetimes of components made from TiAl-based alloys.

For this reason, surface modifications like the so-called "halogen effect" [9-11] as well as overlay coatings [12] can be favorable way to enhance the oxidation resistance independently

from the substrate properties. Potential coatings are based on aluminum (aluminizing) or silicon (siliconizing) as elements that form protective thermally grown oxides of α-Al_2O_3 or SiO_2 [13]. Surface aluminizing of TiAl alloys is based on the formation of $TiAl_3$ which is known to form protective Al_2O_3 [14] and thus is a promising approach. The disadvantage of $TiAl_3$ is its brittleness, which could lead to cracks and spallation when it is applied as a coating material and thus the maximum coating thickness is limited [14, 15]. However, thin $TiAl_3$ layers are easily depleted of Al due to the formation of the thermally grown Al_2O_3 top layer as well as due to interdiffusion processes between coating and substrate material [16, 17].

Surface siliconizing of TiAl alloys leads to the formation of substantial amounts of the Ti_5Si_3 phase which shows a good oxidation resistance [18-20]. A disadvantage of Ti_5Si_3, besides the brittle behavior [20, 21], is the anisotropy of the coefficient of thermal expansion (CTE) which can lead to micro cracks and therefore to an insufficient protection of the base alloy [22, 23]. Additionally, the oxidation behavior of Ti_5Si_3 is considerably affected by interstitial elements and impurities [24].

However, coatings which consist of both Al and Si seem to balance the properties and are promising to increase the oxidation resistance of TiAl. A variety of different technologies and processes has been used to produce these coatings: Al, Ti-98Al and $TiAl_3$ thin films produced by magnetron sputtering [16-18], arc evaporation coatings (Al-10.61Si and Al) [25-27], Al-Si and Al-Si-Y coatings by high speed physical vapor deposition (HS-PVD) [28, 29] cold gas sprayed Al-12Si and Al-20Si [30, 31], slurry coatings (Al-11.95Si) [32] and aluminizing by pack cementation as well as vapor phase aluminizing [33-38].

However, the co-deposition of Al and Si by magnetron sputtering was not reported in literature so far and could be a useful supplement since it allows a precise control over the process and coating composition. In addition, magnetron sputtering enables different coating designs, including multi-component [39] or multilayer coatings [40].

In the present paper, a novel magnetron sputtered Al-18Si (in at.%) coating is introduced. Fundamental investigations were carried out to understand the phase evolution and processes during the required post heat treatment as well as the subsequent oxidation behavior. These studies included *in situ* high temperature x-ray diffraction (HT-XRD) measurements to track the phase evolution during annealing, which allowed the development of a heat treatment for the investigated coatings. Additional, TEM analysis helped to investigate and describe the nanostructure of the coatings after the heat treatment as well as the isothermal oxidation at 850 °C for 300 h.

2. Materials and Methods

The γ-TiAl based alloy TNB-V2 (Al: 45 at.%, Nb: 8 at.%, C: 0.2 at.%;) was used as substrate material. The material was supplied by *GFE – GESELLSCHAFT FÜR ELEKTROMETALLURGIE.* Flat coin samples were produced from an extruded and annealed rod by electric discharge machining with a diameter of 15 mm and a thickness of 1 mm. Additionally, a hole of 1 mm was drilled in each specimen for fixation during the deposition process and the oxidation tests.

For surface finishing the samples were polished by vibratory finishing with a centrifugal disc finishing machine TE 10 HD from *AVATEC*. Prior to coating deposition all samples were cleaned in an ultrasonic bath with ethanol.

The coating was produced by DC magnetron sputtering in an industrial size IMPAX 1000 HT system from *SVS VACUUM COATING TECHNOLOGY*. The specimens were positioned between a pure Al (99.99%) and Si (99.999%) target and turned in a twofold rotation during the sputter process. The chamber was preheated to 200 °C and remained at this temperature during the whole process. Ar was used as process gas and the flow was set to 300 sccm, resulting in a pressure of $5.1*10^{-3}$ mbar. Before the actual deposition process a 15 min plasma etching was performed with a BIAS voltage of -500 V in order to clean the surface. The deposition itself took 4 hours.

A thermal post-treatment was performed during high temperature x-ray diffraction (HT-XRD) measurements in a D8 advanced diffractometer from *BRUKER* equipped with a high temperature oven chamber HTK 1200N from *ANTON PAAR* for an *in-situ* investigation. A temperature of max. 550 °C and a time of 20 h were chosen. The HT-XRD measurements were performed in air as well as in a vacuum atmosphere (< 10^{-4} mbar) and the heating rate was in both cases 5 K/min. Bragg-Brentano geometry was used for HT-XRD as well as for the room temperature XRD measurements where the same diffractometer was utilized.

A scheme of the chamber is illustrated in Fig. 1. For the measurement, the sample is placed on a ceramic carrier where the thermocouple is mounted. In vacuum the sample is only heated by radiation and a thermal gradient occurs within the carrier resulting in a lower measured temperature. When measuring in air, the whole volume within the chamber is heated leading to a homogenous temperature in the carrier and a more accurate temperature measurement. Due to these inaccuracies, the heat treatment in air at 550 °C for 20 h was repeated utilizing a calibrated box furnace N11/H from *NABERTHERM GMBH*. An isothermal oxidation test was performed at 850 °C for 300 h in lab air in the same box furnace.

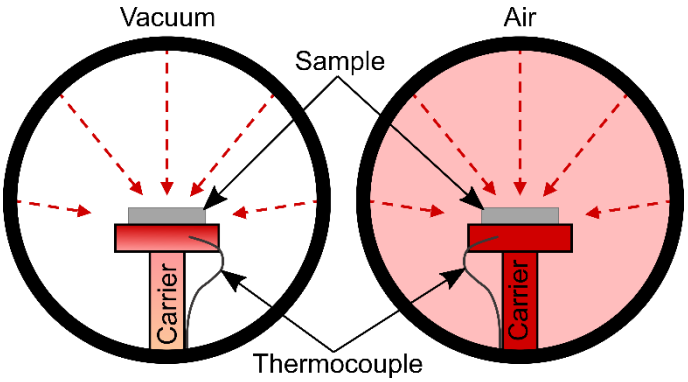

Fig. 1: Simplified scheme of the high-temperature chamber when measuring in vacuum (left) and air (right)

The specimens were analyzed by scanning electron microscopy (SEM) utilizing a *FEI* Helios NanoLab 600i equipped with energy-dispersive X-ray spectroscopy (EDS). The same system was used for preparation of thin lamellas via focused ion beam technique for the analysis using transmission electron microscopy (TEM). The scanning transmission electron microscopy

(STEM) investigations were performed using a *FEI* TITAN 80-300 equipped with X-FEG (Field Emission Gun) operated at 300kV accelerating voltage and EDS detector.

3. Results

3.1. Microstructure of the Al-Si coating after deposition by magnetron sputtering

The Al-Si coating deposited by magnetron sputtering shows a thickness of 11 µm which corresponds to a deposition rate of around 2.75 µm/h. The coating provides good adhesion to the TNB-V2 substrate material. A SEM cross section is presented in Fig. 2a. The coating microstructure consists of small Si grains (< 2µm) with an elongated globular shape embedded in an Al matrix at the lower coating part (3-4 µm) near to the substrate interface, while in the upper coating part the Si grains have a more branched structure.

The corresponding XRD measurement, shows a crystalline coating microstructure of Si and Al phase, see the section presented in Fig. 2b. Some minor peaks of the tetragonal γ-TiAl phase are visible which belong to the substrate material and partially overlap with the Al peaks.

The coating composition after the deposition was 18 at.% Si and 82 at.% Al measured by energy dispersive X-ray spectroscopy using a statistical area scan of the cross section. Neither Ti nor Nb from the TNB-V2 substrate was found within the coating.

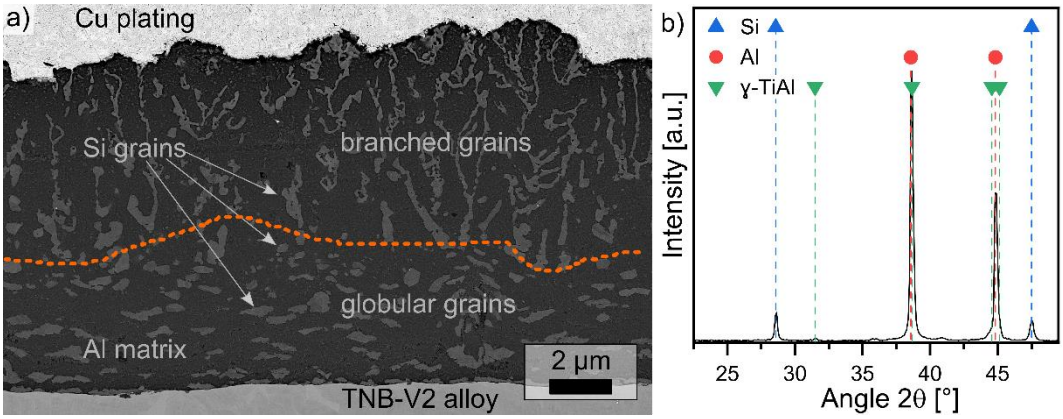

Fig. 2: SEM cross section of the Al-Si coating on a TNB-V2 alloy in the as coated condition which was deposited at 200 °C substrate temperature with the transition line between mostly globular and columnar grained areas (a), and section of the corresponding x-ray diffractogram (b)

3.2. Thermal post-treatments of the Al-18Si (in at.%) magnetron sputtered coating

To obtain high temperature stable phases, a heat treatment in vacuum and lab air was performed in a HT-XRD unit with *in situ* investigation. The corresponding x-ray diffractograms are presented in Fig. 3. The first phase that disappeared due to interdiffusion and phase formation processes between the Al-18Si (in at.%) coating and the TNB-V2 TiAl alloy was the silicon phase. By annealing in a vacuum atmosphere, after 2 hours no silicon reflexes could be detected anymore.

Simultaneously, $TiSi_2$ formed during the heat up and thus the corresponding peak is present after heating to 550 °C. The $TiSi_2$ peak intensity increased slightly during further annealing but eventually disappeared after 5 hours. Due to overlapping peaks it cannot be clearly distinguished in XRD if the present phase is the $TiSi_2$ phase or the related ternary τ_2-$Ti(Al_xSi_{1-x})_2$ phase. However, the following results suggested that the present phase is the ternary τ_2-$Ti(Al_xSi_{1-x})_2$ Phase.

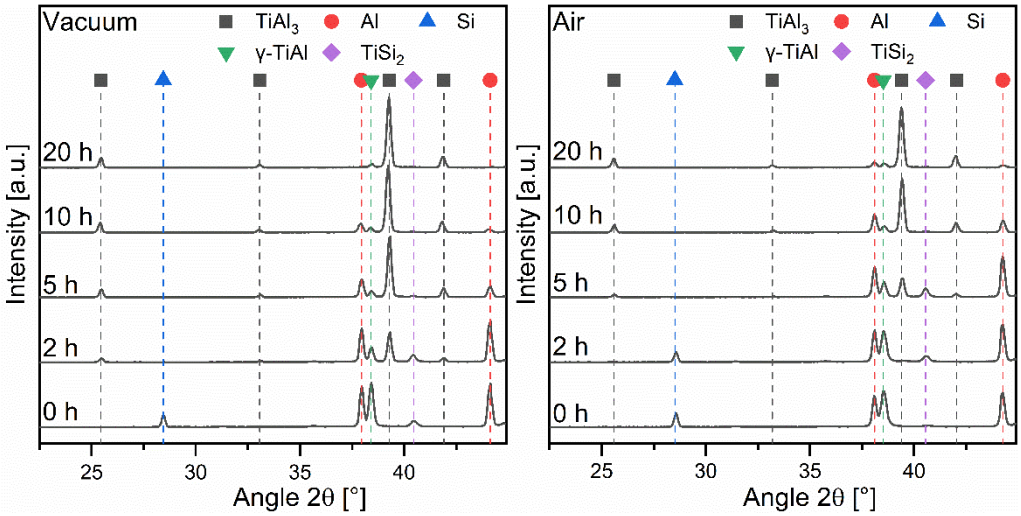

Fig. 3: Sections of high temperature XRD scans performed *in situ* at 550 °C at certain times performed in a vacuum atmosphere (left) and in lab air (right)

It is suggested that Al reacted with the Ti during a longer heat treatment and formed $TiAl_3$. This is represented by the dropping intensities of the Al peaks in the diffractograms, leading finally after 20 h to their disappearance. The Ti was provided by the substrate and the reaction could have taken place by inward diffusion of Al in the substrate as well as outward diffusion of Ti into the coating.

Additionally, at elevated temperatures the γ-TiAl peaks from the substrate material become visible due to the different volumetric changes of pure Al and γ-TiAl phase. The Al peaks are shifted to lower diffraction angles during heat up which causes the separation of the different peaks. Over time, the intensity of the γ-TiAl peaks decreases due to the increase in layer thickness caused by interdiffusion processes between coating and substrate.

After 20 h of heat treatment at 550 °C, the Al peak disappeared and no major changes in the intensity of the remaining peaks are recognizable anymore. A complete transformation of the Al-Si coating into the high temperature stable $TiAl_3$ due to interdiffusion processes could be observed. No Si containing phases were visible in the diffractograms after 20 h. This indicates either a solubility of Si in the measured $TiAl_3$ phase and/or too small dimensions of potential Si containing phases for the detection by XRD. The Al-Si coated TNB-V2 sample which was exposed to air shows a similar but overall slower phase transformation in comparison to the sample which was exposed in a vacuum atmosphere. The reason for the different reaction kinetics is probably related to a discrepancy in the actual and the measured temperature induced by differences in the heat transfer between vacuum and air conditions.

Therefore, the Al-Si coating exposed to vacuum was exposed to slightly higher temperature than the set 550 °C. Since no melting was observed, recognizable by the presence of the Si peak in the diffractograms, the actual temperature was below the Al-Si eutectic temperature of 577 °C [41]. Oxide formation could not be detected in XRD measurements.

SEM analyses of the Al-Si coating on TNB-V2 alloy after 20 h of exposure to 550°C in air and high vacuum atmosphere are presented in Fig. 4. The cross sections reveal an increase in the coating thickness of around 6 µm for the vacuum annealed sample (Fig. 4a) and 4 µm for the air annealed one (Fig. 4b) due to the outward diffusion from Ti and Nb from the TNB-V2 substrate material into the coating as well as Al inwards diffusion into the substrate. The main phase in the coating is the tetragonal $TiAl_3$-phase, as found by XRD, with a Si content of around 9-10 at.%, confirmed by EDS (see Fig. 5). However, since up to 16.4 at.% Si can be dissolved in the $TiAl_3$ phase at 550 °C [42], the Si-rich $TiAl_3$ phase will be denoted as $Ti(Al,Si)_3$. This is confirmed by EDS-line scans that show a Si content of around 9-10 at.% (Fig. 5).
In the vacuum annealed specimen, the shape of the $Ti(Al,Si)_3$ grains varied from globular microstructure at the top of the coating to columnar at the interface between coating and substrate material (Fig. 4a). The sample that was annealed in air in a box furnace shows a comparable microstructure consisting of columnar and globular grains (Fig. 4b). However, at the surface also columnar grains are present. In the middle of the coating the grains are globular. Additionally, an interface between different grain morphologies is present at the upper region of the coating.
A Si-rich phase was formed as a thin interlayer between the coating and the substrate in the air as well as in the vacuum annealed sample (Fig. 4c-d). The thickness of the interlayer was higher for the vacuum annealed sample (~0.5 µm) in comparison with the air annealed sample (~0.2 µm). These interlayers showed a columnar structure. Beside the interlayers, a Si-rich phase was present as grains close to the surface and as small precipitates in the columnar $Ti(Al,Si)_3$ grains after both types of heat treatment.
The EDS line scans exhibited a rather homogeneous elemental distribution along the coating thickness. A slightly higher Si content is detectable close to coating/substrate interface, especially in the Al-Si coating which was exposed to the vacuum atmosphere. This matches with occurrence of the Si-rich interlayer, which was observed in the SEM cross sections (Fig. 4c-d). Oxygen was not found within the coating in the air annealed sample.

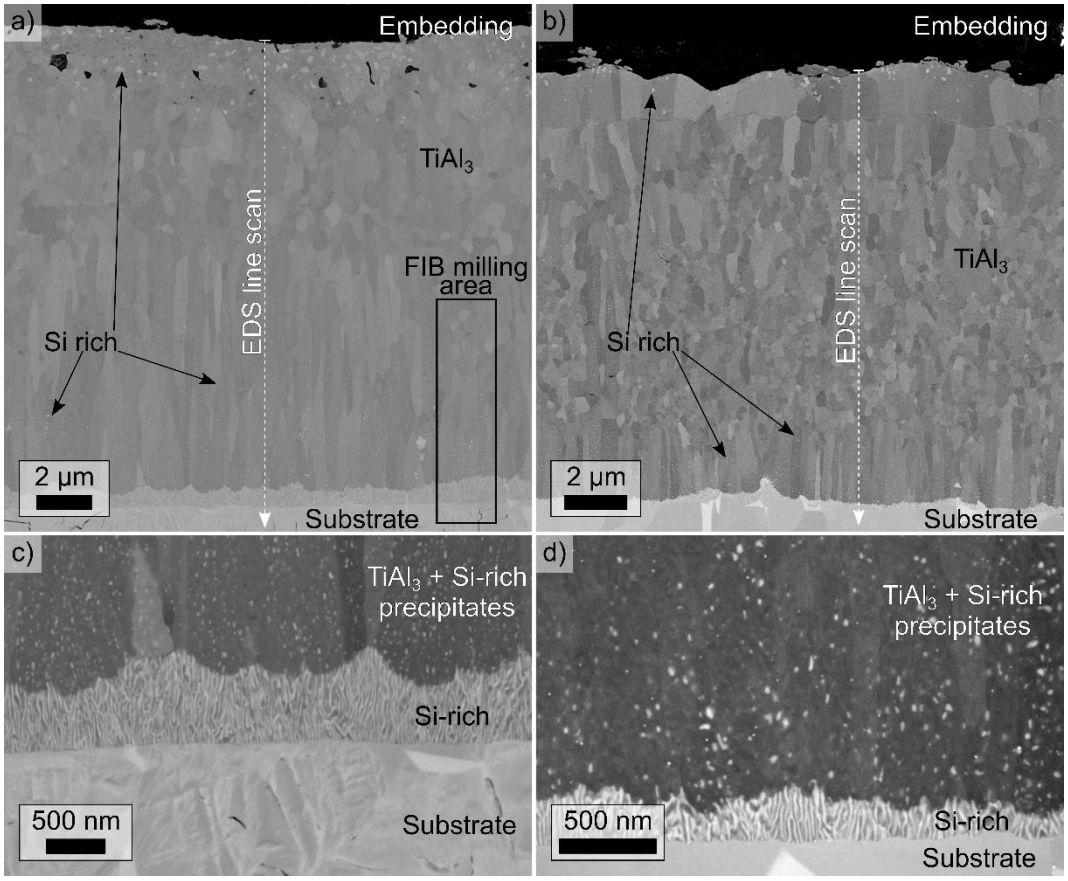

Fig. 4: SEM micrographs of the TNB-V2 samples coated with Al-Si: a) after annealing in vacuum in HT-XRD, b) after annealing in air at 550°C for 20h in a box furnace, Interlayer at the substrate/coating interface of the vacuum (c) and air (d) annealed sample.

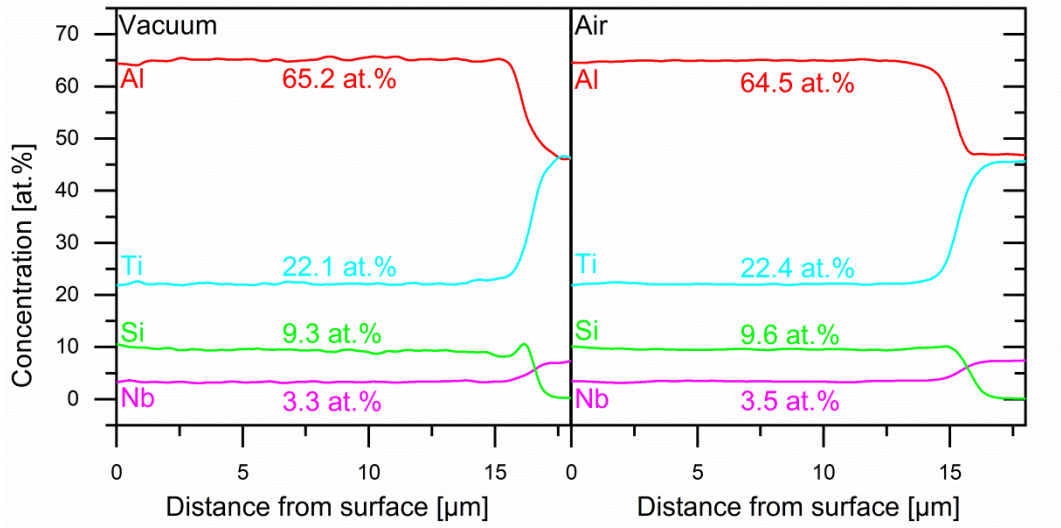

Fig. 5: EDS line scans through the Al-Si coatings on TNB-V2 alloy of the vacuum annealed (left) and air annealed (right) sample

TEM analysis, presented in Fig. 6, was performed to identify the phases and the small Si-rich precipitates. Selected area diffraction (SAD) analysis confirmed the tetragonal $Ti(Al,Si)_3$ as the main present phase (Fig. 6a-b). Moreover, high resolution TEM (HRTEM) investigations revealed the presence of nanometric precipitates distributed uniformly within the $TiAl_3$ phase (Fig. 6c). Since the selected area aperture is not capable of isolating such small precipitates,

Fast Fourier Transform (FFT) was obtained from the precipitate shown in Fig. 6c and allowed to identify it as orthorhombic Ti_5Si_4 (Fig. 6d).

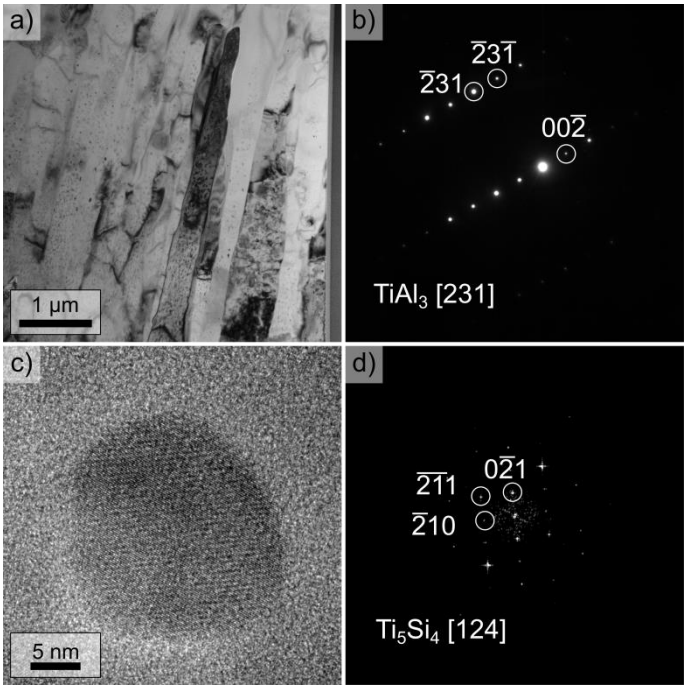

Fig. 6: TEM bright field image of the columnar $TiAl_3$ phase area with Si-rich precipitates (a), corresponding Selected Area Diffraction Pattern (SADP) of the tetragonal $TiAl_3$ phase (b), high resolution TEM (HRTEM) image of a Si-rich precipitate (c) with the corresponding Fast Fourier Transform (FFT) pattern, which reveals the orthorhombic Ti5Si4 phase (d)

In order to understand the phase transformation mechanism, further heat treatment at 550°C in a vacuum atmosphere was conducted in the HT-XRD system but was interrupted after 2 h when $TiSi_2$ peaks become visible. The coating consists of a nearly pure Al top layer of 6-8 µm and the reaction zone of 2-4 µm at the coating/substrate interface which is shown in Fig. 7. The corresponding EDS measurements are summarized in Table 1. The top layer consists of Al and a minor amount of Ti. No Si was detectable in the top layer indicating that all Si reacted with the Ti within the reaction zone at the coating/substrate interface. The $TiSi_2$ phase which was identified in XRD (see Fig. 3) contains a noticeable amount of Al, as found in EDS. This suggests that the present phase is the ternary, orthorhombic τ_2-$Ti(Al_xSi_{1-x})_2$ phase [43-45] since the solubility of Al in $TiSi_2$ is only 0.4 at.% [46]. As mentioned above, the $TiSi_2$ and τ_2-$Ti(Al_xSi_{1-x})_2$ have overlapping peaks and thus cannot be clearly distinguished by XRD. Additionally, a $Ti(Al,Si)_3$ interlayer formed between the substrate and the τ_2-phase. Besides that, a thin Si rich layer is already visible at the $Ti(Al,Si)_3$ substrate interface (Fig. 7b). This layer is comparable to the one which can be observed in the 20 h annealed specimens. Bright precipitates are also visible in the τ_2-$Ti(Al_xSi_{1-x})_2$ as well as in the $Ti(Al,Si)_3$ phase regions(Fig. 7b, c). Due to the elemental contrast of the backscatter electron detector it is very likely that these precipitates

are rich in Si and Ti. This indicates that the orthorhombic Ti_5Si_4 precipitates which are detected after the 20 h annealing were formed during a quite early stage of heat treatment.

Nb was found in the reaction zone as well. In literature a solid solution of $TiAl_3$ and $NbAl_3$ over the complete pseudobinary section was described [47]. Thus, it can be assumed that the Nb is present as $(Ti,Nb)(Al,Si)_3$. No data for the solubility of Nb in τ_2-$Ti(Al_xSi_{1-x})_2$ are available which prevents a final statement on Nb. However, Nb could probably substitute the Ti in the τ_2-phase as well.

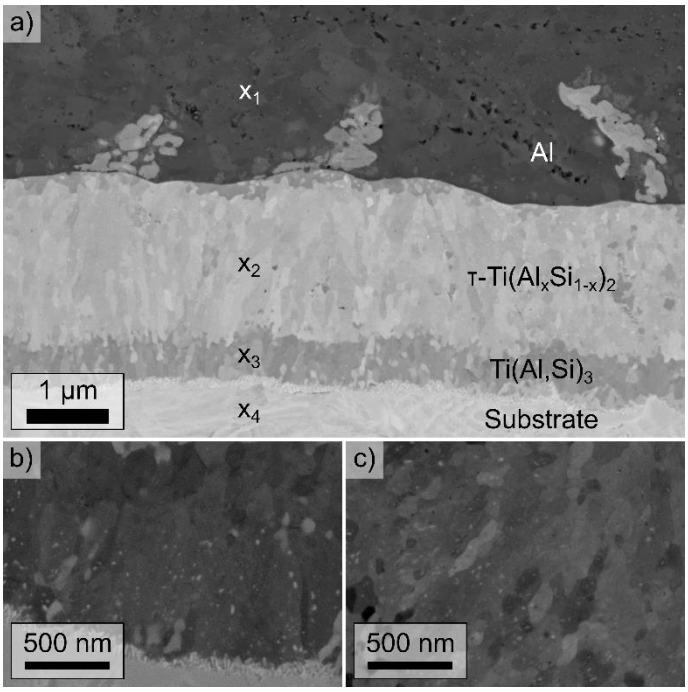

Fig. 7: SEM micrographs of the Al-Si coated specimen after annealing for 2 h at 550 °C in vacuum atmosphere with corresponding the EDS measurements listed in Table 1 and detailed sections of the $Ti(Al,Si)_3$ (a) and τ_2-$Ti(Al_xSi_{1-x})_2$ (b) phase regions

Table 1: EDS measurements of the marked points in Fig. 7 in at.%

Point	Al [at.%]	Si [at.%]	Ti [at.%]	Nb [at.%]
x_1	99.7%	0.0%	0.3%	0.0%
x_2	16.8%	49.2%	29.1%	4.9%
x_3	46.2%	22.5%	26.7%	4.6%
x_4	44.9%	0.0%	46.9%	8.2%

3.3. Oxidation behavior of the Al-Si coating at 850°C for 300h

The Al-Si coated TNB-V2 alloy samples exposed to vacuum and air at 550°C show a similar behavior during the heat treatment. Therefore, in the following section only the vacuum annealed sample will be described in detail.

Isothermal long-term oxidation testing at 850 °C for 300 h in laboratory air shows the development of a hierarchically network-like structure, further referred as network, within the Al-Si coating and a thermally grown oxide (TGO) on top (Fig. 8).

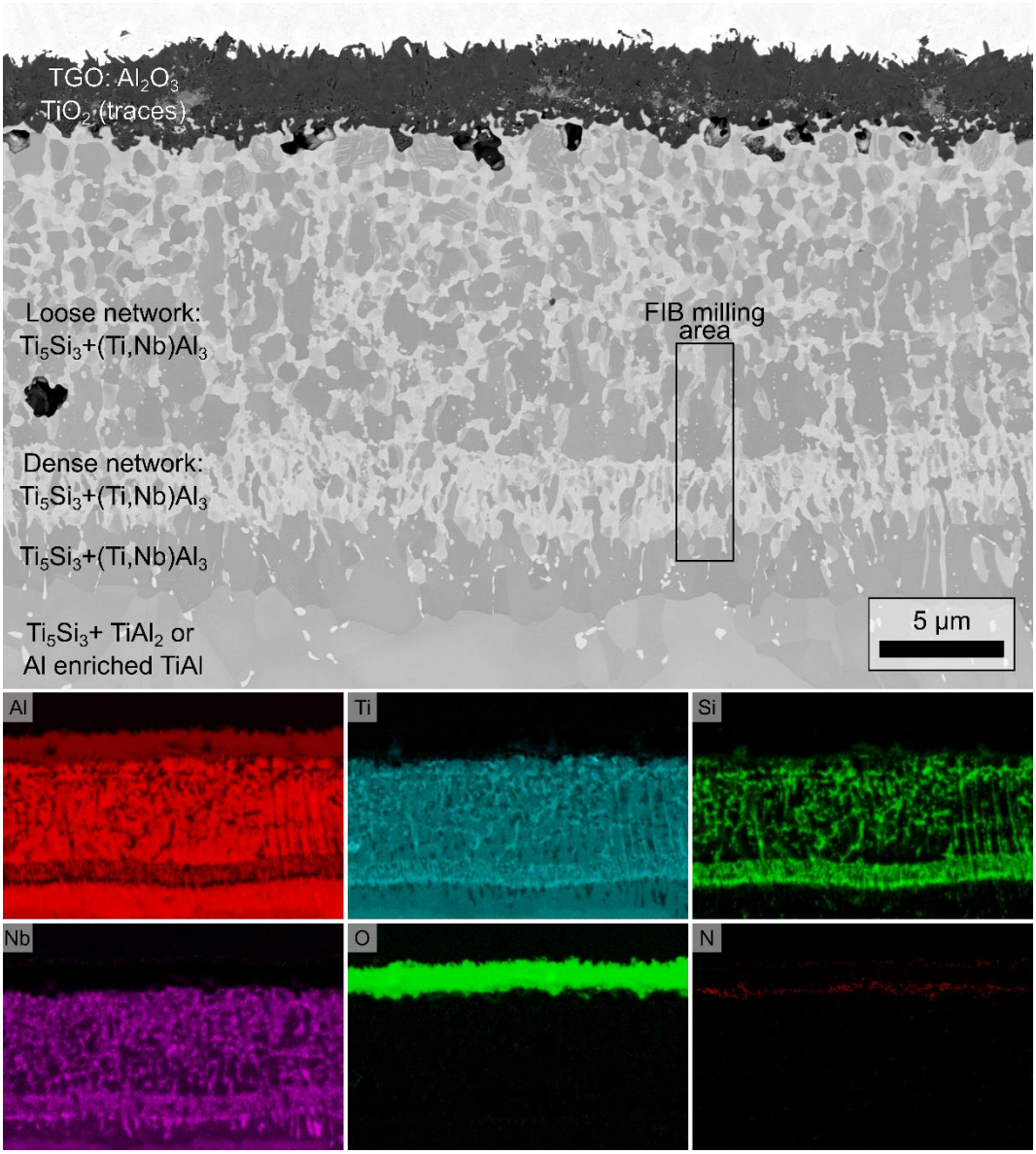

Fig. 8: SEM micrographs of the isothermal oxidized samples (850 °C, 300 h in air) that was thermal post-treatment in vacuum and corresponding EDS element mapping

Considering the EDS element mapping in Fig. 8 and the corresponding XRD diffractogram (Fig. 9), the TGO scale consists mainly of α-Al_2O_3 with some traces of TiO_2. Further, some bright Ti and Si-rich precipitates of probably Ti_5Si_3 are present within the TGO as well as a N-rich layer between the TGO and the Al-Si coating which is visible in the EDS mapping. However, in XRD no nitrides were detected which is due to the small dimensions of this layer. The thickness of the TGO was around 3.3±0.4 µm, as measured in the SEM cross sectional image.

Below the α-Al_2O_3 scale, the coating can be separated into different regions. Directly below the TGO, a network of Ti_5Si_3 has formed that surrounds the Al-rich phases such as $TiAl_2$, $TiAl_3$ and probably partially $NbAl_3$ whereby the majority of the Nb seems to be present within the Ti_5Si_3.

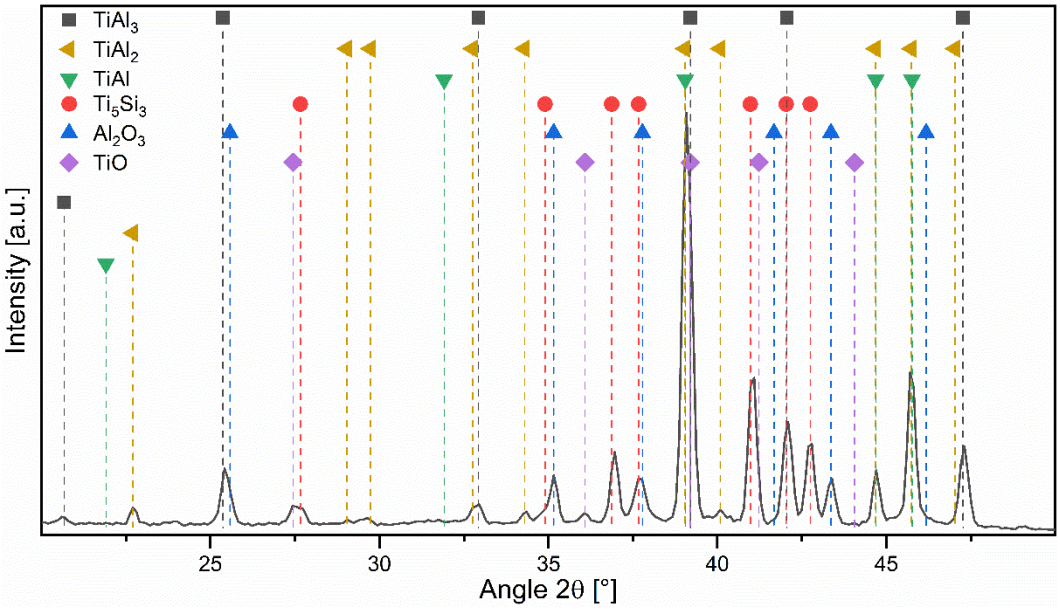

Fig. 9: XRD section of the Al-Si coated TNB-V2 specimen after isothermal exposure to 850 °C for 300 h in lab air.

Additionally, after the oxidation tests small Si-rich precipitations (<500 nm) are still present within the aluminide matrix (Fig. 10a) as well. A TEM-EDS mapping showed that these precipitates are rich in Si and Ti which suggests that those are also the Ti_5Si_3 phase as described in previous work [48]. Additionally, in line with the literature, an uneven distribution of Nb was found within in the Ti_5Si_3 precipitation as well (Fig. 10b).

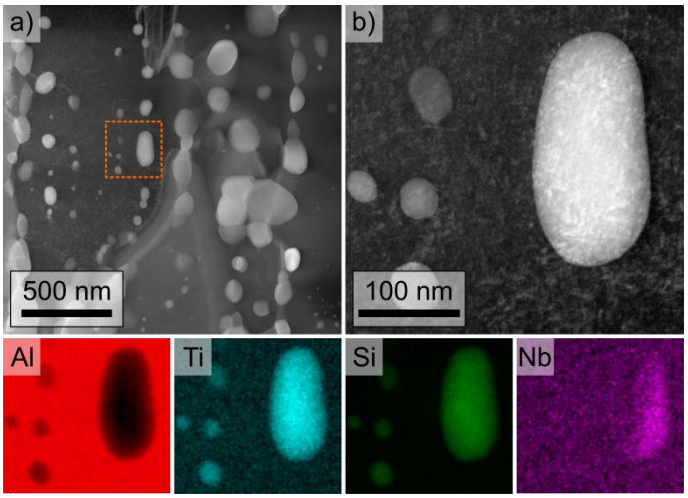

Fig. 10: STEM-HAADF micrograph of the loose network with the Si-rich precipitation from the 300 h at 850 °C isothermal oxidized sample a) as well as the EDS-mapping region with the corresponding element maps b)

Beneath the loose network a denser silicide network is located. Due to the depth from the surface, XRD does not provide sufficient information of the dense silicide network since most of the signal was from the loose region. Therefore, phase identification using TEM was performed in this region (Fig. 11). The results show that also tetragonal $TiAl_3$ and hexagonal Ti_5Si_3 are present, which is in line with the elemental distribution from Fig. 8.

The layer below the dense silicide network is marked by small, isolated silicide precipitations in an Al-rich matrix of probably (Ti,Nb)Al_3

Underneath, a roughly 30-35 µm thick layer of a $TiAl_2$ or an Al-enriched TiAl zone formed due to inward diffusion of Al from the Al-Si coating. Additional silicide grains are sporadically present in that area as well. In summary, it can be stated that in total a range of 50-60 µm below the surface was affected during the oxidation. At greater depths the unchanged TNB-V2 substrate material is still present.

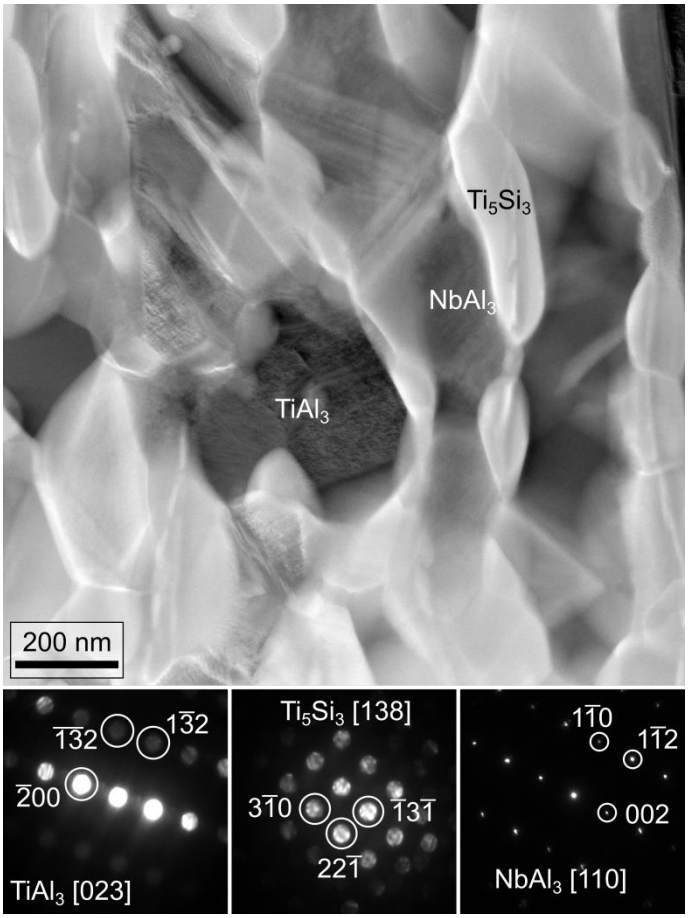

Fig. 11: TEM micrograph of the dense Si-rich network in the Al-Si coating on TBN-V2 after 300h at 850°C in air with the Selected Area Diffraction Pattern (SADP) of the present phases

3.4. Formation of Ti_5Si_3 during oxidation

The reason that Ti_5Si_3 forms during oxidation at 850 °C from $Ti(Al,Si)_3$, but not during the annealing at 550 °C, is the depletion of Al during the oxidation. To illustrate this, Thermo-Calc software [49] was used to calculate the fractions of the phases involved as a function of the Al content (Fig. 12). The analyzed composition corresponds approximately to the composition of the introduced coating. Starting with 100% $TiAl_3$, Ti_5Si_3 formed with decreasing Al content. At the same time, the Si content consequently decreased in the $TiAl_3$ phase. When the maximum amounts of Ti_5Si_3 are formed, $TiAl_3$ transforms to $TiAl_2$. This indicates a very limited solubility of Si in the $TiAl_2$ phase. In literature, only very limited data of the solubility of Si in $TiAl_2$ is

available and is generally referred as very low [31]. Lit et al. determined the maximum solubility of Si in $TiAl_2$ at 700 °C as 1.5 at.% [46]. However, Li et al. [46] achieved a fine $TiAl_3$/$TiAl_2$ eutectoid microstructure and used SEM-EDS to determine the phase composition, which is not capable of measuring very small regions with precision. Therefore, the solubility measurements of Si in $TiAl_2$ do not seem to be free of doubt and might be influenced by the surrounding $TiAl_3$ phase, which would lead to higher results.

The calculations shown in Fig. 12 are in good agreement with the results obtained in [48], where the deposition of a SiAl coating by the pack cementation method at 850 °C resulted in the formation of $TiAl_3$ and Ti_5Si_3 mixture.

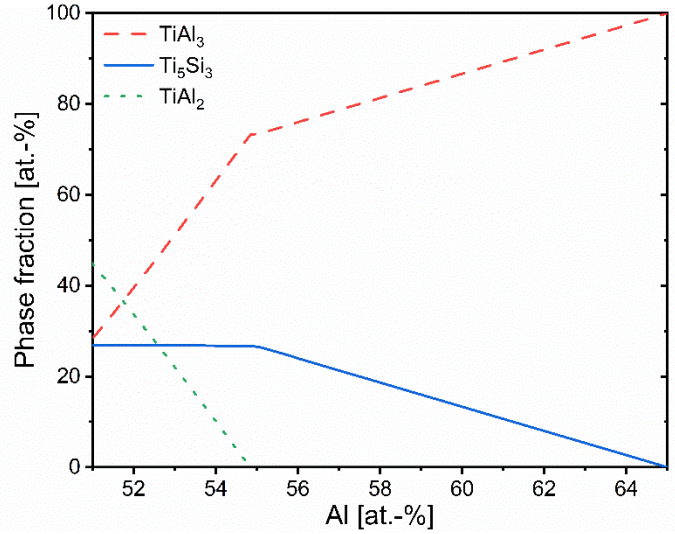

Fig. 12: Phase fractions of a Ti-Al alloy with a constant content of Si (10 at.%) and Nb (3 at.%) at 850 °C as a function of Al. Calculated using Thermo-Calc software [49] with TCTI2 Ti/TiAl-alloys database version 2.2

4. Discussion

4.1. Microstructure formation during deposition process

Magnetron sputtering enables the production of > 10 µm thick Al-18Si (in at.%) coatings on the TiAl-based TNB-V2 alloy. Coating spallation after deposition as described by CHU ET AL. for pure RF magnetron sputtered Al coatings with a coating thicknesses above 5 µm [16] was not observed in the present work. The reason for that could be the heating to 200 °C during the deposition process which could allow stress relieving during the process and therefore preventing spallation.

A similar branched structure of the Si grains within the Al matrix is found in literature for Al-20Si sputtered coatings as well [50, 51]. In the literature, no heating was mentioned so it is suggested that the sputtering took place at room temperature. According to Kucharska et al. [50] the reason for the structure could be that the new deposited Si crystals preferably formed at the already formed Si grains. In the present work, the heating of 200 °C during the deposition process led to Si diffusion to the regions deposited earlier. Therefore, the globular Si grains form close to the substrate/coating interface. In the region below the surface the branched

structure of the Si grains still remains. This indicates that at a temperature of 200 °C Si diffusion within an Al matrix is already possible which agrees with the data given in the literature [52]. However, the absence of Ti or Nb in the coating after the deposition reveals that no diffusion between the coating and TNB-V2 substrate occurred and therefore no intermetallic phases in the sputtered Al-Si coating were formed. The formation of high-temperature stable phases relies on a subsequent heat treatment.

4.2. Heat treatment and phase formation

The temporary formation of the τ_2-$Ti(Al_xSi_{1-x})_2$ phase during heat treatment was also described by Wang et al. for Al-12Si and Al-20Si cold gas sprayed coatings [30]. Additionally, they described the formation of a $Ti(Al,Si)_3$ layer beneath the τ_2-phase during further heat treatment which was also observed in the present study. Thus, it can be concluded that the phase formation takes place according to the mechanism suggested by Wang et al. [30]. According to this, at first a reaction between the TiAl substrate and the inward diffusing Si to the ternary the τ_2-$Ti(Al_xSi_{1-x})_2$ phase take place. Simultaneously, the excess Al from the substrate forms $Ti(Al,Si)_3$ below the τ_2-layer. Afterwards, the τ_2-$Ti(Al_xSi_{1-x})_2$ phase is transformed into the $Ti(Al,Si)_3$ phase by inward diffusing Al from the overlaying Al layer [30].
In the present study, a heat treatment at around 550 °C for 20 h leads to the formation of only $Ti(Al,Si)_3$ and Ti-Si phases such as Ti_5Si_4, which are known to be high temperature stable and oxidation resistant [14, 32].
Heat treatments in air or in vacuum led to similar results. The slightly slower coating-substrate interdiffusion and therefore a delayed phase formation in combination with a lower coating thickness during annealing in air can be explained by the setup of the HT-XRD system. After annealing in the calibrated box furnace, the grains of the Al-18Si coating were observed to be smaller and the interlayer was thinner. Therefore, it is likely that, when annealed in vacuum, the temperature in the HT-XRD system was higher than 550 °C
Apart from this, the independence of the phase formation from the atmosphere allows a heat treatment in air. This facilitates the practical utilization of this protective Al-Si coating for TiAl alloys. However, some pure Al was still detected in the air annealed specimen after 550°C for 20 h. This indicates that the time and/or temperature should be extended to finish the formation of stable phases.
The coating microstructure itself was comparable for both heat treatments and no pronounced oxide layer was detected on the air annealed sample. This can be explained by the formation of a thin Al_2O_3 passivation layer on the Al-Si coating even at room temperature [53]. This oxide layer was too thin to be detected with the used analytic methods but protects the sample at the relatively low temperature of 550 °C against extensive oxidation. Additionally, the temperature is too low for a significant diffusion of oxygen through the oxide layer which therefore prevents oxygen induced embrittlement.
The formation of the Si-rich precipitates of Ti_5Si_4 presumably takes place during the initial phase of the heat treatment. Wang and Chen investigated the formation of titanium silicide

utilizing Ti coated Si wafer [54]. They observed that the silicides form within the amorphous interlayer between the pure Ti layer and Si substrate. On the Si rich side metastable orthorhombic Ti_5Si_4 formed whereas on the Ti rich side Ti_5Si_3 formed. The data in this study suggest that the observed Ti_5Si_4 precipitates were formed during the outward diffusion of Ti from the TNB alloy into the Si grains of the Al-Si coating in the initial state. At the same time Si did also react at the coating/substrate interface by forming Ti_5Si_3 that was identified as a Si-rich layer at the coating/substrate interface. The formation of Ti_5Si_3 is supported by the low solubility of Si in γ-TiAl of only 0.8 at.% at 700 °C [46]. Thus, Si prefers the reaction with Ti from the substrate at the coating/substrate interface rather than the diffusion into the substrate alloy. The precipitates themselves are too small to be detected by XRD using Bragg-Brentano geometry which explains the missing peaks in the diffractograms (see Fig. 3).

4.3. Oxidation behavior

During oxidation, the structure of the Al-Si coating transforms from a homogeneous $Ti(Al,Si)_3$ layer to a hierarchical structure. Wang et al. observed also a structure change in a cold gas sprayed Al-12Si coating on TiAl during oxidation and found a comparable hierarchical microstructure [31]. They described the segregation of the Si from the $Ti(Al,Si)_3$ to the grain boundaries and thus the formation a Si-rich phase. In the present work, a similar behavior was also observed and the Si-rich phase was identified as Ti_5Si_3.

However, due to the higher Si content in the presented initial coating of 18 at.% compared with only 12 at.% in the work by Wang et al. [31] the formation of Ti_5Si_3 is more pronounced leading to the network-like structure. Overall, the higher Si content is responsible for a stronger pronouncement of the different structural features like the dense network. On the other side, a continuous Si-rich layer below the TGO, which was described by Wang et al. [31], was not observed in the present work which could be explained by the lower oxidation temperature of 850 °C in comparison to 900 °C.

It is suggested that the Si content of 18 at.% influences the oxidation behavior in two ways. On the one hand Si could getter Ti by forming Ti_5Si_3. This would prevent the oxidation of Ti and a preferred oxidation of Al is achieved. In the present study, this can be seen by the formation of predominantly protective Al_2O_3 and only a negligible amount of TiO_2 in the TGO.

On the other hand, the formed Ti_5Si_3 network-like structure could act as a diffusion barrier hindering the diffusion of Al to the TNB substrate and thus counteract the depletion of Al in the coating. In fact, a fast consumption of Al as reported in literature for $TiAl_3$ coatings [16, 17, 33, 34] was not observed. On the contrary, after oxidation for 300 h oxidation at 850 °C a significant amount of $TiAl_3$ phase is still present. This leads to the assumption that oxidation protection is retained with further prolonged oxidation which is the topic of ongoing research.

In addition, the TGO was free of cracks and consisted mostly of Al_2O_3 indicating excellent oxidation resistance of the Al-18Si layer. This is due to the fact that $TiAl_3$ forms Al_2O_3 instead of mixed oxides during oxidation [14].

The measured TGO thickness of around 3.3 µm is close to that for similar coatings reported in the literature. Xiang et al. [55] tested pure aluminide ($TiAl_3$) and silicide/aluminide coatings at 850 °C for 240 h. The reported TGO thicknesses were around 4 µm for the former and around 1 µm for the latter coating. Both coatings were produced by pack cementation.
In previous studies, aluminide and Si-aluminide coatings produced by pack cementation were also investigated [56]. The long-term cyclic oxidation at 850 °C led to the formation of 4-5 µm thick oxide scale for a high Si containing coating, 1 µm for a low Si containing coating and over 20 µm for a simple aluminide coating. However, these thicknesses were measured after 3013 h of oxidation at 850 °C. Since the main increase in mass occurs during the first cycles [56], which correlates with the TGO thickness, it can be assumed that the further TGO growth after 300 hours is relatively low. Both studies [55, 56] showed a dependence of the oxidation behavior on the Si content. Thus, the oxidation protection of a magnetron sputtered Al-Si coating could be further increased by adjusting the Si content. Therefore, this will be part of future studies, since magnetron sputtering allows for precise adjustment of the Si content in Al-Si coatings.
EDS element mapping reveals a N-rich region between TGO and the intermetallic part of the coating. Ti_5Si_3 is known to form TiN at low oxygen partial pressures [24, 57]. Tang et al. suggested that Si-deficient and stoichiometric Ti_5Si_3 can solve N interstitially. This led to the formation of nitrides and resulted in a breakaway oxidation [24]. However, Tang et al. also noted that an occupant of interstitial sites, as it occurred in $Ti_5Si_3C_{0.5}$ or $Ti_5Si_{3.2}$, prevent the dissolution of N.
Since in this study the Ti_5Si_3 mainly formed during oxidation from $Ti(Al,Si)_3$ or Ti_5Si_4 it can be assumed that a dissolution of N did not occur in this case. The formation of nitrides is more likely to occurred due to the low oxygen partial pressure underneath the protective alumina TGO in this upper coating layer.

The influence of the presented coating on the mechanical properties is the subject of future investigations. Especially in terms of fatigue strength, protective but brittle coatings are detrimental [58, 59]. On the other hand, oxidation resistant coatings can reduce oxygen uptake and thus counteract the formation of a brittle oxygen enriched zone in TiAl [60]. Additionally, hierarchical structures may have a positive effect on the failure resistance by leading to a tortuous crack growth [61, 62]. Therefore, the observed hierarchical network-like structure consisting of a Ti_5Si_3 network in a $TiAl_3$ matrix could provide a sufficient failure resistance. In addition, the small Si-rich precipitations could also have an influence on the mechanical behavior as well due to interactions with dislocations and/or cracks. Therefore, further investigations regarding mechanical tests are required.

The necessary thermal post-treatments in air or in vacuum revealed a negligible influence of the atmosphere. The oxidation behavior of differently annealed Al-Si coatings on TBN-V2 substrate is comparable. There are minor differences in the thicknesses of the different regions

of the coating but these should not have a major effect. The reason for the different thicknesses could be the higher temperature of the air annealed sample. After the annealing a different thickness was already observed and thus maintained during oxidation. However, annealing in air is preferable due to the simpler process and the possibility to integrate a pre-oxidation after annealing. The pre-oxidation is necessary for the deposition of a potential thermal barrier coating (TBC) to produce a TGO which provides the adhesion between the oxidation protection layer and the TBC.

5. Conclusion

Magnetron sputtering was used to produce an Al-18Si oxidation resistance coating with a rather high deposition rate of 2.75 µm/h. The coatings adhere well to the TiAl substrate and do not spall at a thickness of 11 µm. A subsequent heat treatment at 550 °C for 20 h increases the coating thickness due to diffusion processes. The post heat treatment is essential for the formation of high temperature stable phases. However, the heat treatment can be performed in vacuum or air which results in similar microstructures consisting of $TiAl_3$ and titanium silicide, mostly Ti_5Si_3. During 300 h isothermal oxidation at 850 °C an adherend, thin and dense TGO formed on top of the coating consisting of mainly Al_2O_3 which is the dominant oxidation product of the $TiAl_3$ phase. After 300 h of oxidation there is still a significant amount of $TiAl_3$ in the coating left, thus a protection against further oxidation is ensured. The absence of titanium oxide or silicon oxide suggests that no significant oxidation of the Ti_5Si_3 phase has occurred. Consequently, the phase could act as a diffusion barrier and getter for Ti. Therefore, the Ti_5Si_3 phase could have a major positive influence on the resistance of the coating against oxidation. The microstructure of the coating that forms during oxidation can be described as a hierarchical network-like structure of Ti_5Si_3 and Al-rich Ti-Al phases which could provide promising mechanical properties in terms of fatigue which needs further investigation.

6. Acknowledgment

This work was conducted under the financial support of Deutsche Forschungsgemeinschaft (DFG) under grant Schu1372/6-1. The STEM work was performed in the Framework of the Research Project 2016/23/G/ST5/04128, funded by National Science Centre (NCN), Poland. The authors thank J. Brien and F. Kreps for the scientific and technical support at the German Aerospace Center as well as U. Schulz and V. Volkmer for comments that greatly improved the manuscript.

[1] H. Clemens and S. Mayer, "Design, Processing, Microstructure, Properties, and Applications of Advanced Intermetallic TiAl Alloys," vol. 15, no. 4, pp. 191-215, 2013.

[2] F. Appel, J. D. H. Paul, and M. Oehring, *Gamma Titanium Aluminides Alloys – Science and Technology*. Weinheim: Wiley-VCH Verlag, 2011.

[3] A. Lasalmonie, "Intermetallics: Why is it so difficult to introduce them in gas turbine engines?," *Intermetallics*, vol. 14, no. 10, pp. 1123-1129, 2006/10/01/ 2006.

[4] M. P. Brady, W. J. Brindley, J. L. Smialek, and I. E. Locci, "The oxidation and protection of gamma titanium aluminides," *JOM*, vol. 48, no. 11, pp. 46-50, 1996/11/01 1996.

[5] H. Clemens and W. Smarsly, "Light-Weight Intermetallic Titanium Aluminides – Status of Research and Development," *Advanced Materials Research*, vol. 278, pp. 551-556, 2011.
[6] R. Swadźba, K. Marugi, and Ł. Pyclik, "STEM investigations of γ-TiAl produced by additive manufacturing after isothermal oxidation," *Corrosion Science*, vol. 169, p. 108617, 2020/06/01/ 2020.
[7] B. P. Bewlay, S. Nag, A. Suzuki, and M. J. Weimer, "TiAl alloys in commercial aircraft engines," *Materials at High Temperatures*, vol. 33, no. 4-5, pp. 549-559, 2016/06/28 2016.
[8] "Forged Intermetallic γ-TiAl Based Alloy Low Pressure Turbine Blade in the Geared Turbofan," in *Proceedings of the 13th World Conference on Titanium*, pp. 1223-1227.
[9] A. Donchev, R. Braun, and M. Schütze, "Optimizing thermally grown oxide for thermal barrier coatings on TiAl components via fluorine treatment," *JOM*, vol. 62, no. 1, pp. 70-74, 2010/01/01 2010.
[10] A. Donchev and M. Schütze, "Improving the oxidation resistance of γ-titanium aluminides by halogen treatment," vol. 59, no. 6, pp. 489-493, 2008.
[11] M. Schütze *et al.*, "The halogen effect in the oxidation of intermetallic titanium aluminides," *Corrosion Science*, vol. 44, no. 2, pp. 303-318, 2002/02/01/ 2002.
[12] R. Pflumm, S. Friedle, and M. Schütze, "Oxidation protection of γ-TiAl-based alloys – A review," *Intermetallics*, vol. 56, pp. 1-14, 2015.
[13] K. L. Luthra, "Stability of protective oxide films on Ti-base alloys," *Oxidation of Metals*, vol. 36, no. 5, pp. 475-490, 1991/12/01 1991.
[14] J. L. Smialek, "Oxidation behaviour of TiAl3 coatings and alloys," *Corrosion Science*, vol. 35, no. 5, pp. 1199-1208, 1993/01/01/ 1993.
[15] Q. Wang *et al.*, "Improved oxidation performance of TiAl alloy by a novel Al–Si composite coating," *Surface and Coatings Technology*, vol. 381, p. 125126, 2020/01/15/ 2020.
[16] M. S. Chu and S. K. Wu, "The improvement of high temperature oxidation of Ti–50Al by sputtering Al film and subsequent interdiffusion treatment," *Acta Materialia*, vol. 51, no. 11, pp. 3109-3120, 2003/06/27/ 2003.
[17] M. S. Chu and S. K. Wu, "Oxidation Behavior of Ti-50Al Intermetallics with Thin TiAl3 Film at 1000°C," *Oxidation of Metals*, journal article vol. 63, no. 1-2, pp. 1-13, February 01 2005.
[18] M. Fröhlich, A. Ebach-Stahl, R. Braun, and C. Leyens, "Oxidation protective coatings for γ-TiAl – recent trends," *Materialwissenschaft und Werkstofftechnik*, vol. 38, no. 9, pp. 667-673, 2007.
[19] X. Y. Li, S. Taniguchi, Y. Matsunaga, K. Nakagawa, and K. Fujita, "Influence of siliconizing on the oxidation behavior of a γ-TiAl based alloy," *Intermetallics*, vol. 11, no. 2, pp. 143-150, 2003/02/01/ 2003.
[20] R. Rosenkranz, G. Frommeyer, and W. Smarsly, "Microstructures and properties of high melting point intermetallic Ti5Si3 and TiSi2 compounds," in *High Temperature Aluminides and Intermetallics*, S. H. Whang, D. P. Pope, and C. T. Liu, Eds. Oxford: Elsevier, 1992, pp. 288-294.
[21] G. Frommeyer and R. Rosenkranz, "Microstructures and Properties of the Refractory Silicides Ti5Si3 and TiSi2 and Ti-Si-(Al) Eutectic Alloys," in *Metallic Materials with High Structural Efficiency*, Dordrecht, 2004, pp. 287-308: Springer Netherlands.
[22] J. H. Schneibel and C. J. Rawn, "Thermal expansion anisotropy of ternary titanium silicides based on Ti5Si3," *Acta Materialia*, vol. 52, no. 13, pp. 3843-3848, 2004/08/02/ 2004.
[23] A. J. Thom, M. K. Meyer, Y. Kim, and M. Akinc, *Evaluation of A5Si3Zx intermetallics for use as high temperature structural materials*. United States: Minerals, Metals ampersand Materials Society, 1994.
[24] Z. Tang, J. J. Williams, A. J. Thom, and M. Akinc, "High temperature oxidation behavior of Ti5Si3-based intermetallics," *Intermetallics*, vol. 16, no. 9, pp. 1118-1124, 2008/09/01/ 2008.
[25] L. Swadzba, G. Moskal, M. Hetmanczyk, B. Mendala, and G. Jarczyk, "Long-term cyclic oxidation of Al–Si diffusion coatings deposited by Arc-PVD on TiAlCrNb alloy," *Surface and Coatings Technology*, vol. 184, no. 1, pp. 93-101, 2004.
[26] L. Swadzba, A. Maciejny, B. Mendala, G. Moskal, and G. Jarczyk, "Structure and resistance to oxidation of an Al–Si diffusion coating deposited by Arc-PVD on a TiAlCrNb alloy," *Surface and Coatings Technology*, vol. 165, no. 3, pp. 273-280, 2003/02/17/ 2003.
[27] F. A. Varlese, M. Tului, S. Sabbadini, F. Pellissero, M. Sebastiani, and E. Bemporad, "Optimized coating procedure for the protection of TiAl intermetallic alloy against high temperature oxidation," *Intermetallics*, vol. 37, pp. 76-82, 2013/06/01/ 2013.
[28] K. Bobzin, T. Brögelmann, C. Kalscheuer, and T. Liang, "Al-Si and Al-Si-Y coatings deposited by HS-PVD for the oxidation protection of γ-TiAl," *Surface and Coatings Technology*, vol. 350, pp. 587-595, 2018/09/25/ 2018.
[29] K. Bobzin, T. Brögelmann, C. Kalscheuer, T. Liang, C. H., and K. H., "Thermal cyclic oxidation behavior of γ-TiAl with in situ post-annealed Al-Si-Y coating," vol. 37, no. 4, p. 041401, 2019.
[30] J. Wang, L. Kong, T. Li, and T. Xiong, "Microstructure Evolution of Cold-Sprayed Al-Si Alloy Coatings on γ-TiAl During Heat Treatment," *Journal of Thermal Spray Technology*, vol. 24, no. 6, pp. 1071-1080, 2015/08/01 2015.
[31] J. Wang, L. Kong, J. Wu, T. Li, and T. Xiong, "Microstructure evolution and oxidation resistance of silicon-aluminizing coating on γ-TiAl alloy," *Applied Surface Science*, vol. 356, pp. 827-836, 2015/11/30/ 2015.
[32] M. Goral, L. Swadzba, G. Moskal, M. Hetmanczyk, and T. Tetsui, "Si-modified aluminide coatings deposited on Ti46Al7Nb alloy by slurry method," *Intermetallics*, vol. 17, no. 11, pp. 965-967, 2009.

[33] H. G. Jung and K. Y. Kim, "Effect of ternary elements on the oxidation behavior of aluminized TiAl alloys," *Oxidation of Metals*, Article vol. 58, no. 1-2, pp. 197-216, 2002/08/01 2002.
[34] V. Gauthier, F. Dettenwanger, M. Schütze, V. Shemet, and W. J. Quadakkers, "Oxidation-Resistant Aluminide Coatings on γ-TiAl," *Oxidation of Metals*, journal article vol. 59, no. 3, pp. 233-255, April 01 2003.
[35] R. Braun, M. Fröhlich, C. Leyens, and D. Renusch, "Oxidation Behaviour of TBC Systems on γ-TiAl Based Alloy Ti–45Al–8Nb," *Oxidation of Metals*, vol. 71, no. 5-6, pp. 295-318, 2009/03/12 2009.
[36] T. C. Munro and B. Gleeson, "The deposition of aluminide and silicide coatings on γ-TiAl using the halide-activated pack cementation method," (in English), *Metallurgical and Materials Transactions A: Physical Metallurgy and Materials Science*, Article vol. 27, no. 12, pp. 3761-3772, 1996.
[37] M. Goral, L. Swadzba, G. Moskal, G. Jarczyk, and J. Aguilar, "Diffusion aluminide coatings for TiAl intermetallic turbine blades," *Intermetallics*, vol. 19, no. 5, pp. 744-747, 2011/05/01/ 2011.
[38] Z. D. Xiang, S. R. Rose, and P. K. Datta, "Codeposition of Al and Si to form oxidation-resistant coatings on γ-TiAl by the pack cementation process," *Materials Chemistry and Physics*, vol. 80, no. 2, pp. 482-489, 2003.
[39] R. Anton, V. Leisner, P. Watermeyer, M. Engstler, and U. Schulz, "Hafnia-doped silicon bond coats manufactured by PVD for SiC/SiC CMCs," *Acta Materialia*, vol. 183, pp. 471-483, 2020/01/15/ 2020.
[40] C. Maurer and U. Schulz, "Solid particle erosion of thick PVD coatings on CFRP," *Wear*, vol. 317, no. 1, pp. 246-253, 2014/09/15/ 2014.
[41] J. L. Murray and A. J. McAlister, "The Al-Si (Aluminum-Silicon) system," *Bulletin of Alloy Phase Diagrams*, vol. 5, no. 1, p. 74, 1984/02/01 1984.
[42] J. Wang, Y. Liu, Y. Liu, C. Wu, and X. Su, "The Isothermal Section of the Al-Si-Ti Ternary System at 550 °C," *Journal of Phase Equilibria and Diffusion*, vol. 40, no. 6, pp. 810-819, 2019/12/01 2019.
[43] O. Dezellus, B. Gardiola, J. Andrieux, M. Lomello-Tafin, and J. C. Viala, "On the Liquid/Solid Phase Equilibria in the Al-Rich Corner of the Al-Si-Ti Ternary System," *Journal of Phase Equilibria and Diffusion*, vol. 35, no. 2, pp. 137-145, 2014/04/01 2014.
[44] Q. Luo, Q. Li, J.-Y. Zhang, S.-L. Chen, and K.-C. Chou, "Experimental investigation and thermodynamic calculation of the Al–Si–Ti system in Al-rich corner," *Journal of Alloys and Compounds*, vol. 602, pp. 58-65, 2014/07/25/ 2014.
[45] S. P. Gupta, "Intermetallic compounds in diffusion couples of Ti with an Al–Si eutectic alloy," *Materials Characterization*, vol. 49, no. 4, pp. 321-330, 2002/11/01/ 2002.
[46] Z. Li *et al.*, "700 °C Isothermal Section of the Al-Ti-Si Ternary Phase Diagram," *Journal of Phase Equilibria and Diffusion*, vol. 35, no. 5, pp. 564-574, 2014/10/01 2014.
[47] V. Raghavan, "Al-Nb-Ti (Aluminum-Niobium-Titanium)," *Journal of Phase Equilibria and Diffusion*, vol. 26, no. 4, pp. 360-368, 2005/10/01 2005.
[48] R. Swadźba *et al.*, "Characterization of Si-aluminide coating and oxide scale microstructure formed on γ-TiAl alloy during long-term oxidation at 950 °C," *Intermetallics*, vol. 87, pp. 81-89, 2017.
[49] J. O. Andersson, T. Helander, L. Höglund, P. Shi, and B. Sundman, "Thermo-Calc & DICTRA, computational tools for materials science," *Calphad*, vol. 26, no. 2, pp. 273-312, 2002/06/01/ 2002.
[50] B. Kucharska and J. Kowalczyk, "Resistance Properties of Al-Si Coatings," *Acta Physica Polonica A*, vol. 129, no. 2, pp. 197-199, 02/01 2016.
[51] B. Kucharska and A. Wróbel-Knysak, "The mechanical properties of AlSi coatings made by PVD technology," *Mechanik*, no. 1, pp. 66-67, 2017.
[52] G. J. van Gurp, "Diffusion-limited Si precipitation in evaporated Al/Si films," *Journal of Applied Physics*, vol. 44, no. 5, pp. 2040-2050, 1973/05/01 1973.
[53] V. K. Agarwala and T. Fort, "Nature of the stable oxide layer formed on an aluminum surface by work function measurements," *Surface Science*, vol. 54, no. 1, pp. 60-70, 1976/01/01/ 1976.
[54] M. H. Wang and L. J. Chen, "Phase formation in the interfacial reactions of ultrahigh vacuum deposited titanium thin films on (111)Si," *Journal of Applied Physics*, vol. 71, no. 12, pp. 5918-5925, 1992/06/15 1992.
[55] Z. D. Xiang, S. R. Rose, and P. K. Datta, "Oxidation resistance of diffusion coatings formed by pack-codeposition of Al and Si on γ-TiAl," *Journal of Materials Science*, vol. 39, no. 6, pp. 2099-2106, 2004/03/01 2004.
[56] R. Swadźba, L. Swadźba, B. Mendala, P.-P. Bauer, N. Laska, and U. Schulz, "Microstructure and cyclic oxidation resistance of Si-aluminide coatings on γ-TiAl at 850 °C," *Surface and Coatings Technology*, vol. 403, p. 126361, 2020/12/15/ 2020.
[57] Z. Tang, A. J. Thom, and M. Akinc, "Role of nitrogen on the oxidative stability of Ti5Si3 based alloys at elevated temperature," *Intermetallics*, vol. 14, no. 5, pp. 537-543, 2006/05/01/ 2006.
[58] N. Laska and R. Braun, "Oxidation and fatigue behaviour of gamma titanium aluminides coated with yttrium or zirconium containing intermetallic Ti–Al–Cr layers and thermal barrier coating," *Materials at High Temperatures*, vol. 32, no. 1-2, pp. 221-229, 2015/01/01 2015.
[59] R. Braun, N. Laska, S. Knittel, and U. Schulz, "Effect of intermetallic coatings on the tensile properties of a γ-TiAl based TNM alloy," *Materials Science and Engineering: A*, vol. 699, pp. 118-127, 2017/06/24/ 2017.
[60] M. Schütze, "The Role of Surface Protection for High-Temperature Performance of TiAl Alloys," *JOM*, vol. 69, no. 12, pp. 2602-2609, 2017/12/01 2017.

[61] J. Suryawanshi, K. G. Prashanth, S. Scudino, J. Eckert, O. Prakash, and U. Ramamurty, "Simultaneous enhancements of strength and toughness in an Al-12Si alloy synthesized using selective laser melting," *Acta Materialia,* vol. 115, pp. 285-294, 2016/08/15/ 2016.

[62] S. A. Hosseini, P. Moretti, D. Konstantinidis, and M. Zaiser, "Beam network model for fracture of materials with hierarchical microstructure," *International Journal of Fracture,* vol. 227, no. 2, pp. 243-257, 2021/02/01 2021.